Chaos, Solitons and Fractals 181 (2024) 114719

Contents lists available at ScienceDirect

Chaos, Solitons and Fractals

journal homepage: www.elsevier.com/locate/chaos

Bound-in-continuum-like corner states in the type-II Dirac photonic lattice

Suge Feng [a], Hua Zhong [a], Milivoj R. Belić [b], Dumitru Mihalache [c], Yongdong Li [a], Yiqi Zhang [a,*]

[a] Key Laboratory for Physical Electronics and Devices, Ministry of Education, School of Electronic Science and Engineering, Xi'an Jiaotong University, Xi'an 710049, China

[b] Division of Arts and Sciences, Texas A&M University at Qatar, P.O. Box 23874 Doha, Qatar

[c] Horia Hulubei National Institute of Physics and Nuclear Engineering, 077125 Magurele, Bucharest, Romania

ARTICLE INFO

Keywords:
Type-II Dirac cone
Corner state
Bound state in continuum

ABSTRACT

Dirac points are special points in the energy band structure of various materials, around which the dispersion is linear. If the corresponding Fermi surface is projected as a pair of crossing lines—or touching cones in two dimensions, the Dirac point is known as the type-II; such points violate the Lorentz invariance. Until now, thanks to its unique characteristics, the Klein tunneling is successfully mimicked and the topological edge solitons are obtained in the type-II Dirac photonic lattices that naturally possess type-II Dirac points. However, the interplay between these points and corner states is still not investigated. Here, we report both linear and nonlinear corner states in the type-II Dirac photonic lattice with elaborate boundaries. The states, classified as in-phase and out-of-phase, hide in the extended bands that are similar to the bound states in the continuum (BIC). We find that the nonlinear BIC-like corner states are remarkably stable. In addition, by removing certain sites, we establish the fractal Sierpiński gasket structure in the type-II Dirac photonic lattice, in which the BIC-like corner states are also demonstrated. The differences between results in the fractal and nonfractal lattices are rather small. Last but not least, the corner breather states are proposed. Our results provide a novel view on the corner states and may inspire fresh ideas on how to manipulate/control the localized states in different photonic lattices.

1. Introduction

Dirac points – or Dirac cones – are peculiar structures that appear in the energy band zones of various photonic lattices and topological insulators that describe unusual electronic transport properties in these metamaterials. They indicate the existence of massless fermionic or bosonic particles in the man-made or rare materials in nature that naturally display linear dispersion in the momentum space [1]. The most famous material that possesses Dirac points is the graphene [2], an allotrope of carbon arranged in a single layer of atoms that paved the way to novel two-dimensional (2D) materials and brought revolutionary breakthroughs in the various branches of science.

One has to note that the Dirac point in graphene is type-I, so that the corresponding Fermi-surface is a point. If the Dirac point is tilted sufficiently to make the Fermi-surface appear as a pair of crossing lines, then the type-II Dirac point is obtained [3–9]. Since the existence of type-II Dirac cones violates the Lorentz symmetry, it is rare to find natural materials that possess them. In photonics however, man-made lattices can be elaborately designed to display type-II Dirac cones naturally [10]. This is a quite unique situation that provides an ideal platform for inspecting quasi-particle-mediated phenomena that, for example, might exist in high energy physics but are not directly accessible to experimental verification. However, they naturally appear and can be easily tested in simple optical bench systems with artificially produced photonic lattices.

One the other hand, the type-II Dirac photonic lattices are also attractive for investigating nontrivial topological phenomena, like topological edge solitons [11,12]. To date, topological edge solitons are still experimentally elusive, even though there are many theoretical studies [11–27]. Admittedly, there are some related experimental works reported [11,28,29] but they do not contain the direct observation of topological edge states; the clear experimental observation of such physical objects is still missing.

In contrast to topological edge solitons, nonlinear corner states and corner solitons in higher-order topological insulators [30,31] have been reported both theoretically [24,32–35] and experimentally [36–39]. Until now, most of the higher-order topological insulators reported are based on a few specific lattices, such as honeycomb [40], kagome [36,41,42], the 2D Su–Schrieffer–Heeger [37,39] or even fractal lattices [43–45], but not in type-II Dirac lattices. We wonder – and

* Corresponding author.
E-mail address: zhangyiqi@xjtu.edu.cn (Y. Zhang).

https://doi.org/10.1016/j.chaos.2024.114719
Received 2 January 2024; Received in revised form 2 March 2024; Accepted 9 March 2024

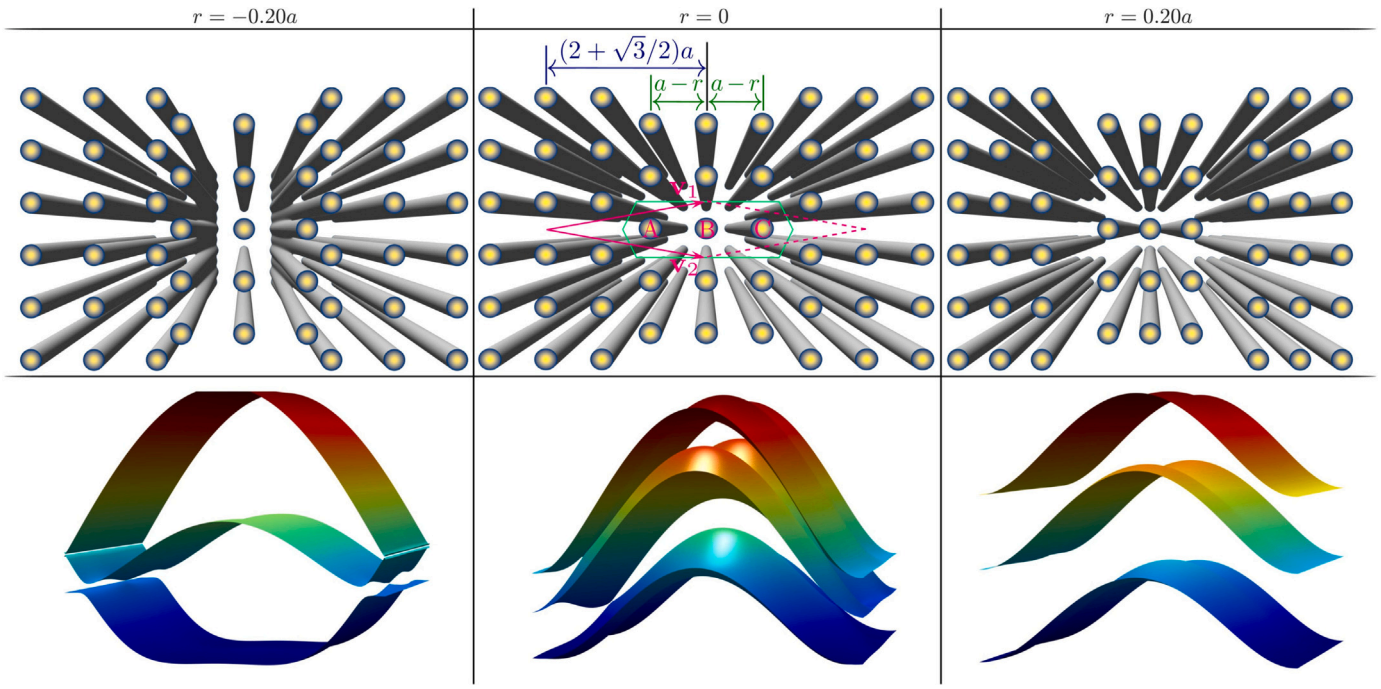

Fig. 1. Type-II Dirac lattice waveguide arrays with different r and their corresponding band structures. There are three sites labeled as A, B, and C in each unit cell (indicated by a green hexagon). The basis vectors of the Bravais lattice are $\mathbf{v}_1$ and $\mathbf{v}_2$, a is the lattice constant and r is the shift parameter. (For interpretation of the references to color in this figure legend, the reader is referred to the web version of this article.)

investigate here – whether corner states can be obtained in these lattices or not. Indeed, this is an intriguing question that is not addressed anywhere up to now, to the best of our knowledge.

In this work, we address this question and give positive answers on the existence of both linear and nonlinear corner states in the specially prepared type-II Dirac photonic lattice. We produce a design with proper cutting edges in the type-II lattice, which supports corner states. In addition, we extend the design to the fractal dimension and form a Sierpiński gasket lattice that also supports corner states. We will show that there exist no explicit bandgaps that may support gap solitons, but these states hide in the extended bands, which makes them quite similar to the bound-in-continuum (BIC) states [46,47]. We believe that the corner states reported in this work are quite different from the previous examples of corner states, in this manner replenishing and refreshing the understanding of such states.

2. Lattice waveguide array and spectrum

The type-II Dirac photonic lattice array is displayed in Fig. 1, in which the unit cell is indicated by a green hexagon that includes three sites marked with A, B, and C. The typical basis vectors are

$$\mathbf{v}_1 = \left[2+\frac{\sqrt{3}}{2}, +\frac{1}{2}\right]a, \quad \mathbf{v}_2 = \left[2+\frac{\sqrt{3}}{2}, -\frac{1}{2}\right]a, \tag{1}$$

with a being the lattice constant. We assume that the unit cells are fixed but the separation between the three sites in each unit cell can be changed. To this end, we introduce a shift parameter r, as shown in Fig. 1: the three sites get closer if $r > 0$ and further away if $r < 0$. In Fig. 1, we also show two lattices with $r = \pm 0.2a$, in addition to the case with $r = 0$. In this manner, waveguide arrays can be formed in the lattice. The lattice waveguide array can be theoretically described by Gaussian functions, as follows

$$\mathcal{R}(x,y) = \sum_{m,n} p \exp\left(-\frac{(x-x_m)^2}{d_1^2} - \frac{(y-y_n)^2}{d_2^2}\right), \tag{2}$$

where (x_m, y_n) is the site coordinate that should weave through all sites, p is the site depth, and $d_{1,2}$ represent the site width. On the right-hand-side of Eq. (2), the site locations are independent of z, so the waveguide array is straight. If one adopts the femtosecond laser direct writing technique for inscribing waveguide arrays in fused silica [36,38,39], the values for these parameters can be chosen as $a = 2$, $d_1 = d_2 = 0.5$, and $p = 8$, which correspond to 20 μm, 5 μm, and the refractive index change of $\sim 8.8 \times 10^{-4}$, if the utilized wavelength is $\lambda = 800$ nm and the normalization parameter is $r_0 = 10$ μm.

The propagation dynamics of light beams in the shallow waveguide array is described by the well-known nonlinear Schrödinger-like paraxial wave equation

$$i\frac{\partial \psi}{\partial z} = -\frac{1}{2}\left(\frac{\partial^2}{\partial x^2} + \frac{\partial^2}{\partial y^2}\right)\psi - \mathcal{R}(x,y)\psi - |\psi|^2\psi, \tag{3}$$

where ψ is the complex envelope of the light beam, and z is the normalized propagation distance. The solutions of Eq. (3), known as the Bloch waves, can be written in the form $\psi = u(x,y)\exp(ibz)$, with $u(x,y)$ being the periodic real function describing the mode profile and b being the propagation constant. Inserting this general solution into Eq. (3), one obtains the following eigenvalue equation

$$bu = \frac{1}{2}\left(\frac{\partial^2}{\partial x^2} + \frac{\partial^2}{\partial y^2}\right)u + \mathcal{R}(x,y)u + |u|^2 u, \tag{4}$$

which can be solved numerically using many methods, for example, the plane-wave expansion or the finite-difference method, to obtain the spectrum of the lattice. Without considering the self-focusing nonlinearity term, the band structures corresponding to the lattices from Fig. 1 in the upper row are shown in the bottom row. For the case with $r = 0$, one can see the type-II Dirac cones that connect each two neighbored bands. While for the cases with $r \neq 0$, the lattice is strained or stretched [48] and the corresponding band structure changes. Numerical simulations demonstrate that the Dirac cones move to the center/boundary of the Brillouin zone if r becomes negative/positive (not shown here). For the case with $r = 0.2a$, all Dirac cones disappear and are replaced by band gaps, since all Dirac cones cross with each other and annihilate. We should point out that the Dirac points here are different from the Dirac

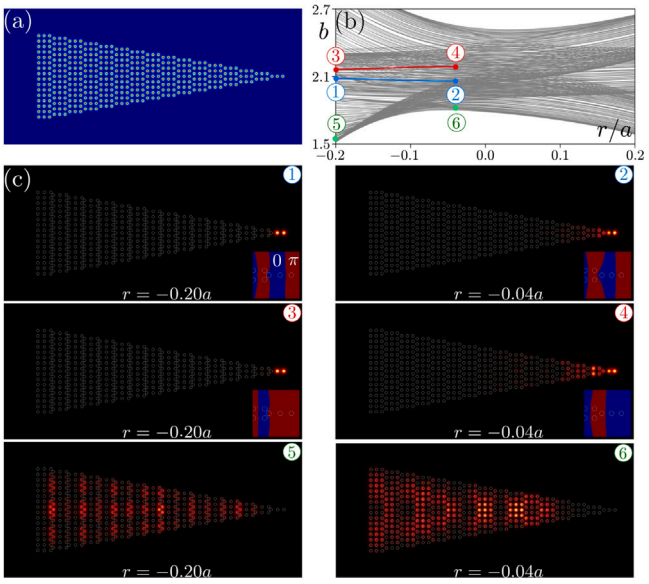

Fig. 2. (a) Type-II Dirac photonic lattice with a triangular landscape. (b) The corresponding spectrum b versus r of the lattice in (a). The red and blue lines represent corner states. (c) Modulus profiles of the selective states in (b) with the corresponding phase distributions given in the inset. White circles represent lattice sites and the insets show phases of the corner states. Blue and red colors represent 0 and π phases, respectively. (For interpretation of the references to color in this figure legend, the reader is referred to the web version of this article.)

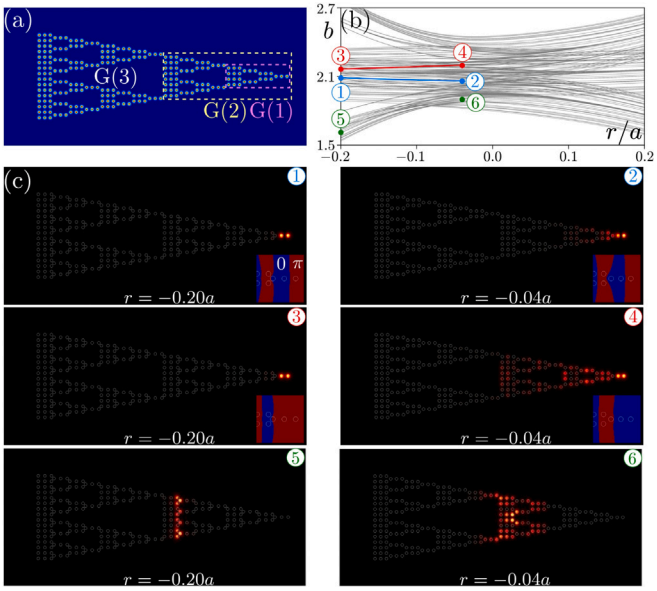

Fig. 3. Setup is as in Fig. 2, but for the fractal G(3) Sierpiński gasket based on the type-II Dirac photonic lattice. The first and second generations G(1) and G(2) of the lattice are marked by the magenta and yellow dashed rectangles. (For interpretation of the references to color in this figure legend, the reader is referred to the web version of this article.)

points embedded in the continuum [49], which are resulting from the coincidence of two BICs at the same Fermi arc.

In this work, we consider two different landscapes for the waveguide array. The first one is given in Fig. 2(a), and is called the triangular array. The spectrum of the lattice, given by the graph of the propagation constant b versus the shift parameter r, is displayed in Fig. 2(b). One sees that there is no explicit band gap in the spectrum and all states strongly mix with each other. We note that the spectrum in Fig. 2(b) is a not a projection of its 2D counterpart, since the configuration in Fig. 2(a) is well isolated and without periodicity. However, one can identify localized corner states hidden within the extended band, by scanning the states one by one for a fixed r. An example is indicated by the red and blue line states, which do not blend with any bulk states. Different from the previous findings that only one part of the localized corner states is within the extended band [37,50–52], the corner states here are totally immersed in the extended band. Therefore, we call them BIC-like corner states. It is a simple task to check the inverse form-factor [53] of all modes, which demonstrates that the width of the corner states is the smallest (not shown here).

We choose two states from the red line and another two from the blue line, which are numbered 1, 2, 3, and 4, respectively. The modulus profiles of these states are exhibited in Fig. 2(c), with the associated phase distributions shown in the inset of each panel. Even though all the states are in the extended band, their localization can be manipulated by the shift parameter r. The bigger the absolute value of r, the better the localization. This property is similar to that of the corner states located in the band gap [34]. By checking the phase of the corner states, one finds that the rightmost two spots are out-of-phase for the states from the blue line and in-phase for the states from the red line. Since the rightmost three sites are similar to those of a trimer chain [54–56], the phase distributions here are also similar to those of the trimer lattice. For comparison, we also show two extended states, numbered 5 and 6 in Fig. 2(c). Except for the two corner states indicated by the blue and red lines in Fig. 2(b) that are localized at the right corner of the structure, we do not find any other corner states, even after checking all possible eigenmodes.

The second landscape considered in this work is the fractal Sierpiński gasket with the generation order 3, as shown in Fig. 3. As is usual with any fractal gasket, they are formed by eliminating certain arrays from a nonfractal lattice and repeating the procedure ad infinitum. We follow the procedure described in [45], with a slight modification (see Fig. 3.) The first generation G(1) and the second generation G(2) of the fractal lattice here are indicated by two dashed rectangles. It is not difficult to see that the nth generation Sierpiński gasket possesses 3^{n+1} sites. Similar to other investigations of the fractal Sierpiński gasket lattices [45,57,58], the Hausdorff dimension of the fractal lattice is $d = \log_2 3$, since the subsequent generation needs three previous generations and the size of the $(n + 1)$th generation becomes two times larger than that of the nth generation. Our "fractal" gasket is just a modified G(3); still, as evident from the visual inspection of Figs. 2(b) and 3(b), many of the bulk states are already eliminated in the G(3) lattice. It is also worth noting that the fractal gasket considered here lacks the C_3 discrete rotational symmetry, which is distinct from the previous Sierpiński gaskets.

By adjusting the shift parameter r, the spectrum of our gasket is displayed in Fig. 3(b). The spectrum is still quite messy, akin to the nonfractal counterpart from above. After scanning the eigenmodes for a given r, one obtains the corner states in the extended band, as indicated by the red and blue lines, which hide in the extended bands. Similar to the operations in Fig. 2, we select four states from the red and blue lines (marked with 1, 2, 3, and 4) as well as two extended states (marked with 5 and 6), and show their amplitude modulus distributions in Fig. 3(c). It is interesting to note that as compared with the corner states of the triangular lattice in Fig. 2(c), the corner states in the fractal lattice still hold most of the properties of the former, even though the insulating bulk is absent. For example, the corner states on the blue line are still out-of-phase, while those on the red line are in-phase. The probable reason is that the corner states are mainly distributed on the rightmost two corner sites, which are far away from the holes of the fractal lattice—the separation between the rightmost unit cell and its nearest hole is the length of one unit cell. However, the localization of the corner state is a bit worse in the fractal lattice if r is close to zero, especially for the in-phase corner states. The close similarity between the results in Figs. 2(c) and 3(c) demonstrates the robustness of the corner states in the system based on the type-II Dirac photonic lattice.

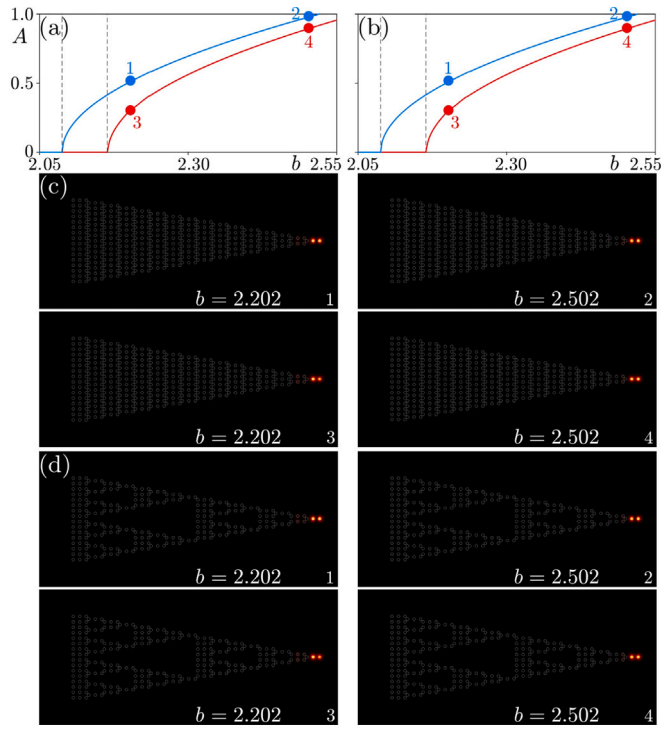

Fig. 4. Nonlinear state families and modulus profiles of the selective nonlinear corner states for $r = -0.2a$. All nonlinear corner states are stable. (a) Peak amplitude of the nonlinear corner state A vs. the propagation constant b in the nonfractal lattice. Blue curve is for the out-of-phase case, while the red curve is for the in-phase case. (b) Results for the fractal lattice. Blue curve is for the out-of-phase case, while the red curve is for the in-phase case. (c) Modulus profiles of the selected nonlinear corner states in (a). (d) Modulus profiles of the selected nonlinear corner states in (b). (For interpretation of the references to color in this figure legend, the reader is referred to the web version of this article.)

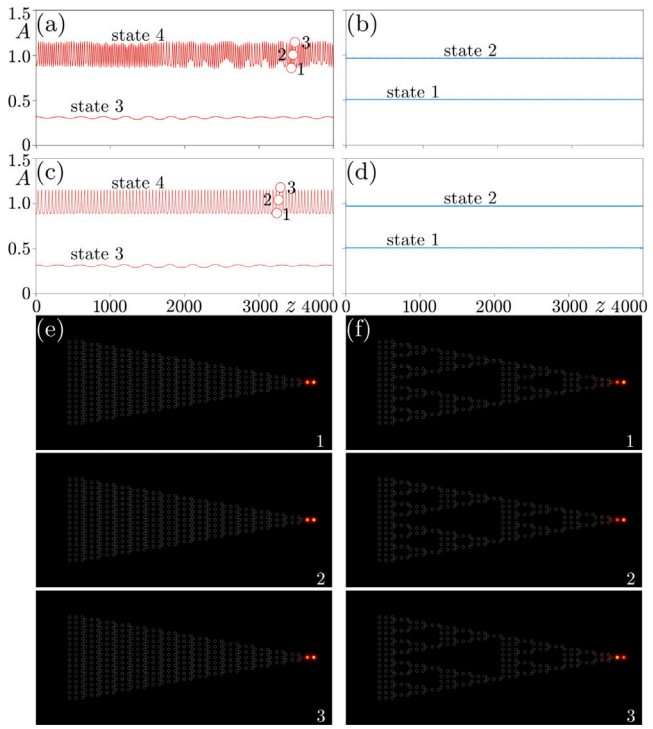

Fig. 5. (a,b) Peak amplitudes of the nonlinear corner states from Fig. 4(a) during propagation in the nonfractal lattice. (c,d) Setup is the same as in (a,b) but for the fractal lattice from Fig. 4(b). (e) Modulus profiles of the state during propagation, corresponding to the dots 1, 2, and 3 in (a). (f) Setup is as in (e) but corresponding to the dots 1, 2, and 3 from (c).

3. Nonlinear corner states

One should keep in mind that the influence of nonlinearity in shallow waveguides is assumed to be small. Then, one can form the energy band structure of the linear lattice and introduce the effects of nonlinearity as a modulation on the underlying band structure. Hence, by directly solving the nonlinear Schrödinger Eq. (4), using, e.g., Newton's iteration method, one can generally obtain the nonlinear localized corner states. Since the corner states lie in the bulk band, as shown in Figs. 2(b) and 3(b), the nonlinear corner states, in the conventional sense, may hybridize with the bulk states and loose their localization. However, in this section we demonstrate that this hybridization does not happen, and the nonlinear corner states are still well localized.

The results differentiating the nonlinear corner states from the linear states at $r = -0.2a$ are displayed in Fig. 4. The nonlinear state families – as recorded in the relation between the peak amplitude $A = \max\{|\psi|\}$ and the propagation constant b – are shown in Figs. 4(a) and 4(b), respectively. They correspond to the in-phase (red curves) and out-of-phase (blue curves) corner states in the nonfractal and fractal type-II Dirac photonic lattices. It is worth mentioning that the nonlinear corner state families are nearly independent of the lattice landscapes, since the families are almost unchanged in the triangular and fractal lattices. From each family, we select two nonlinear corner states and show their modulus distributions in Figs. 4(c) and 4(d). At this point, it is necessary to point out to two interesting properties reflected by our results. The first one is that the localization of the nonlinear corner states is almost unaffected by the increase in the propagation constant (see the amplitude modulus distributions indicated with numbers 2 and 4). The second property is the remarkable stability of these nonlinear corner states.

The stability of the BIC-like nonlinear corner states is investigated by adding a small-scale perturbation (10% of the amplitude) and performing a long-distance propagation (up to $z \sim 4000$). Quite unexpectedly, we find that all the nonlinear corner states are stable, both in the nonfractal and fractal lattice arrays. To display the stability in a more clear way, we choose four nonlinear corner states in the triangular lattice array and record their peak amplitudes A during propagation. The peak amplitudes of states numbered 3 and 4 in Fig. 4(a) are shown in Fig. 5(a), while those corresponding to states numbered 1 and 2 are shown in Fig. 5(b). The states numbered 3 and 4, which are in-phase, exhibit an oscillating behavior, and this phenomenon is more pronounced if the peak amplitude is bigger (see the state 4). However, the out-of-phase nonlinear corner states in Fig. 5(b) do not oscillate. For the in-phase corner states, the energy may couple between the two outermost sites and this is the reason why it oscillates during propagation. Since the oscillation holds even after a long-distance propagation, $z \sim 4000$, the in-phase corner state is regarded as a stable object. To see whether it couples with other modes, we check the projection of the nonlinear corner state onto other linear eigenmodes during propagation, via $p_n(z) = \iint \psi^*(z) u_n dx dy$ with n being the index of linear eigenmodes. We find that the weight of the two linear corner states is the biggest in the nonlinear corner state, while those of other eigenstates are negligible (not shown here).

Similar results are obtained in the fractal lattice array, as shown in Figs. 5(c) and 5(d). For the oscillating case, we show the amplitude modulus profiles at three typical distances, as indicated by three dots in Figs. 5(a) and 5(c), and in Figs. 5(e) and 5(f). The oscillation is due to the fact that the energy of the state couples between the rightmost two sites, which is much easier for the beam with two in-phase humps. The oscillating nonlinear corner state represents a *nonlinear corner breather*.

4. Conclusion

Summarizing, we have investigated both linear and nonlinear corner states in type-II Dirac photonic lattice arrays, by adjusting the separations among three sites in each unit cell. We investigated nonfractal and fractal lattices. Regardless of whether the lattice array was fractal or not, the corner states are always hidden in the extended bands, which makes them BIC-like. We find these BIC-like corner states, both linear and nonlinear, not to hybridize with the extended states and well localized. After comparing the results in nonfractal and fractal arrays, we find them not much different, which indicates that these BIC-like corner states are not affected much by the insulating bulk, which may help the fabrication of potential optical functional devices with fewer channels. Last but not least, the stability of corner states turned out to be rather remarkable, although the existence of corner breathers was also unveiled. We believe these results provide a new viewpoint on corner states and may inspire new ideas for light manipulations in the field of photonic lattice arrays.

Funding

Natural Science Basic Research Program of Shaanxi Province, China (2024JC-JCQN-06). National Natural Science Foundation of China (12074308, 12304370). Fundamental Research Funds for the Central Universities (sxzy012024146). Qatar National Research Fund (project NPRP13S-0121-200126).

CRediT authorship contribution statement

Suge Feng: Writing – original draft, Investigation. **Hua Zhong:** Writing – original draft, Investigation. **Milivoj R. Belić:** Writing – review & editing, Writing – original draft, Investigation. **Dumitru Mihalache:** Writing – review & editing, Writing – original draft, Investigation. **Yongdong Li:** Supervision, Investigation. **Yiqi Zhang:** Writing – review & editing, Writing – original draft, Supervision, Investigation, Formal analysis, Conceptualization.

Declaration of competing interest

The authors declare that they have no known competing financial interests or personal relationships that could have appeared to influence the work reported in this paper.

Data availability

Data will be made available on request.

References

[1] Leykam D, Desyatnikov AS. Conical intersections for light and matter waves. Adv Phys X 2016;1:101–13.
[2] Geim AK, Novoselov KS. The rise of graphene. Nat Mater 2007;6(3):183–91.
[3] Soluyanov A, Gresch D, Wang Z, Wu Q, Troyer M, Dai X, et al. Type-II Weyl semimetals. Nature 2015;527(7579):495–8.
[4] Pyrialakos GG, Nye NS, Kantartzis NV, Christodoulides DN. Emergence of type-II Dirac points in graphynelike photonic lattices. Phys Rev Lett 2017;119:113901.
[5] Mann CR, Sturges TJ, Weick G, Barnes WL, Mariani E. Manipulating type-I and type-II Dirac polaritons in cavity-embedded honeycomb metasurfaces. Nature Commun 2018;9(1):2194.
[6] Hu C, Li Z, Tong R, Wu X, Xia Z, Wang L, et al. Type-II Dirac photons at metasurfaces. Phys Rev Lett 2018;121:024301.
[7] Milićević M, Montambaux G, Ozawa T, Jamadi O, Real B, Sagnes I, et al. Type-III and tilted Dirac cones emerging from flat bands in photonic orbital graphene. Phys Rev X 2019;9:031010.
[8] Pyrialakos GG, Schmitt N, Nye NS, Heinrich M, Kantartzis NV, Szameit A, et al. Symmetry-controlled edge states in the type-II phase of Dirac photonic lattices. Nature Commun 2020;11(1):2074.
[9] Wu X, Li X, Zhang RY, Xiang X, Tian J, Huang Y, et al. Deterministic scheme for two-dimensional type-II Dirac points and experimental realization in acoustics. Phys Rev Lett 2020;124:075501.
[10] Jin KC, Zhong H, Li YD, Ye FW, Zhang YP, Li FL, et al. Parametric type-II Dirac photonic lattices. Adv Quant Technol 2020;3(7):2000015.
[11] Zhong H, Xia S, Zhang Y, Li Y, Song D, Liu C, et al. Nonlinear topological valley Hall edge states arising from type-II Dirac cones. Adv Photon 2021;3(5):056001.
[12] Tian Y, Zhang Y, Li Y, Belić MR. Vector valley Hall edge solitons in the photonic lattice with type-II Dirac cones. Front Phys (Beijing) 2022;17(5):53503.
[13] Lumer Y, Plotnik Y, Rechtsman MC, Segev M. Self-localized states in photonic topological insulators. Phys Rev Lett 2013;111:243905.
[14] Ablowitz MJ, Cole JT. Tight-binding methods for general longitudinally driven photonic lattices: Edge states and solitons. Phys Rev A 2017;96:043868.
[15] Leykam D, Chong YD. Edge solitons in nonlinear-photonic topological insulators. Phys Rev Lett 2016;117:143901.
[16] Gulevich DR, Yudin D, Skryabin DV, Iorsh IV, Shelykh IA. Exploring nonlinear topological states of matter with exciton-polaritons: Edge solitons in kagome lattice. Sci Rep 2017;7(1):1780.
[17] Kartashov YV, Skryabin DV. Modulational instability and solitary waves in polariton topological insulators. Optica 2016;3(11):1228–36.
[18] Li C, Ye F, Chen X, Kartashov YV, Ferrando A, Torner L, et al. Lieb polariton topological insulators. Phys Rev B 2018;97:081103.
[19] Zhang YQ, Kartashov YV, Ferrando A. Interface states in polariton topological insulators. Phys Rev A 2019;99:053836.
[20] Ivanov SK, Kartashov YV, Szameit A, Torner L, Konotop VV. Vector topological edge solitons in Floquet insulators. ACS Photon 2020;7(3):735–45.
[21] Ivanov SK, Kartashov YV, Maczewsky LJ, Szameit A, Konotop VV. Edge solitons in Lieb topological Floquet insulator. Opt Lett 2020;45(6):1459–62.
[22] Ivanov SK, Kartashov YV, Maczewsky LJ, Szameit A, Konotop VV. Bragg solitons in topological Floquet insulators. Opt Lett 2020;45(8):2271–4.
[23] Ivanov SK, Kartashov YV, Heinrich M, Szameit A, Torner L, Konotop VV. Topological dipole Floquet solitons. Phys Rev A 2021;103:053507.
[24] Ren B, Wang H, Kompanets VO, Kartashov YV, Li Y, Zhang Y. Dark topological valley Hall edge solitons. Nanophoton 2021;10(13):3559–66.
[25] Tang Q, Ren B, Kompanets VO, Kartashov YV, Li Y, Zhang Y. Valley Hall edge solitons in a photonic graphene. Opt Express 2021;29(24):39755–65.
[26] Tang Q, Ren B, Belić MR, Zhang Y, Li Y. Valley Hall edge solitons in the kagome photonic lattice. Romanian Rep Phys 2022;74:504.
[27] Tang Q, Zhang Y, Kartashov YV, Li Y, Konotop VV. Vector valley Hall edge solitons in superhoneycomb lattices. Chaos Solitons Fractals 2022;161:112364.
[28] Mukherjee S, Rechtsman MC. Observation of Floquet solitons in a topological bandgap. Science 2020;368(6493):856–9.
[29] Maczewsky LJ, Heinrich M, Kremer M, Ivanov SK, Ehrhardt M, Martinez F, et al. Nonlinearity-induced photonic topological insulator. Science 2020;370(6517):701–4.
[30] Xie B, Wang HX, Zhang X, Zhan P, Jiang JH, Lu M, et al. Higher-order band topology. Nat Rev Phys 2021;3(7):520–32.
[31] Lin ZK, Wang Q, Liu Y, Xue H, Zhang B, Chong Y, et al. Topological phenomena at defects in acoustic, photonic and solid-state lattices. Nat Rev Phys 2023;5(8):483–95.
[32] Hadad Y, Soric JC, Khanikaev AB, Alù A. Self-induced topological protection in nonlinear circuit arrays. Nat Electron 2018;1(3):178–82.
[33] Zangeneh-Nejad F, Fleury R. Nonlinear second-order topological insulators. Phys Rev Lett 2019;123:053902.
[34] Zhang Y, Kartashov YV, Torner L, Li Y, Ferrando A. Nonlinear higher-order polariton topological insulator. Opt Lett 2020;45(17):4710–3.
[35] Zhong H, Kartashov YV, Li Y, Zhang Y. π-Mode solitons in photonic Floquet lattices. Phys Rev A 2023;107:L021502.
[36] Kirsch MS, Zhang Y, Kremer M, Maczewsky LJ, Ivanov SK, Kartashov YV, et al. Nonlinear second-order photonic topological insulators. Nat Phys 2021;17(9):995–1000.
[37] Hu Z, Bongiovanni D, Jukić D, Jajtić E, Xia S, Song D, et al. Nonlinear control of photonic higher-order topological bound states in the continuum. Light Sci Appl 2021;10(1):164.
[38] Ren B, Arkhipova AA, Zhang Y, Kartashov YV, Wang H, Zhuravitskii SA, et al. Observation of nonlinear disclination states. Light Sci Appl 2023;12(1):194.
[39] Arkhipova AA, Zhang Y, Kartashov YV, Zhuravitskii SA, Skryabin NN, Dyakonov IV, et al. Observation of π solitons in oscillating waveguide arrays. Sci Bull 2023;68(18):2017–24.
[40] Noh J, Benalcazar WA, Huang S, Collins MJ, Chen KP, Hughes TL, et al. Topological protection of photonic mid-gap defect modes. Nature Photon 2018;12(7):408–15.
[41] El Hassan A, Kunst FK, Moritz A, Andler G, Bergholtz EJ, Bourennane M. Corner states of light in photonic waveguides. Nature Photon 2019;13(10):697–700.
[42] Zhang Y, Bongiovanni D, Wang Z, Wang X, Xia S, Hu Z, et al. Realization of photonic p-orbital higher-order topological insulators. eLight 2023;3(1):5.
[43] Li J, Mo Q, Jiang JH, Yang Z. Higher-order topological phase in an acoustic fractal lattice. Sci Bull 2022;67(20):2040–4.
[44] Zheng S, Man X, Kong ZL, Lin ZK, Duan G, Chen N, et al. Observation of fractal higher-order topological states in acoustic metamaterials. Sci Bull 2022;67(20):2069–75.
[45] Ren B, Kartashov YV, Maczewsky LJ, Kirsch MS, Wang H, Szameit A, et al. Theory of nonlinear corner states in photonic fractal lattices. Nanophoton 2023;12(19):3829–38.

[46] Hsu CW, Zhen B, Stone AD, Joannopoulos JD, Soljačić M. Bound states in the continuum. Nat Rev Mater 2016;1(9):16048.
[47] Kang M, Liu T, Chan CT, Xiao M. Applications of bound states in the continuum in photonics. Nat Rev Phys 2023;5(11):659–78.
[48] Ren B, Wang H, Belić MR, Li Y, Zhu X, Zhang Y. Zero-energy edge states and solitons in strained photonic graphene. Phys Rev A 2023;107:043504.
[49] Pujol-Closa P, Artigas D. Dirac points embedded in the continuum. Phys Rev B 2023;108:205106.
[50] Benalcazar WA, Cerjan A. Bound states in the continuum of higher-order topological insulators. Phys Rev B 2020;101:161116.
[51] Cerjan A, Jörg C, Vaidya S, Augustine S, Benalcazar WA, Hsu CW, et al. Observation of bound states in the continuum embedded in symmetry bandgaps. Sci Adv 2021;7(52):eabk1117.
[52] Li C, Kartashov YV, Konotop VV. Topological Floquet bound states in the continuum. Opt Lett 2022;47(19):5160–3.
[53] Zhang Y, Kartashov YV, Zhang Y, Torner L, Skryabin DV. Inhibition of tunneling and edge state control in polariton topological insulators. APL Photon 2018;3(12):120801.
[54] Zhang Y, Ren B, Li Y, Ye F. Topological states in the super-SSH model. Opt Express 2021;29(26):42827–36.
[55] Kartashov YV, Arkhipova AA, Zhuravitskii SA, Skryabin NN, Dyakonov IV, Kalinkin AA, et al. Observation of edge solitons in topological trimer arrays. Phys Rev Lett 2022;128:093901.
[56] Shen S, Kartashov YV, Li Y, Zhang Y. Floquet edge solitons in modulated trimer waveguide arrays. Phys Rev Appl 2023;20:014012.
[57] Xu XY, Wang XW, Chen DY, Smith CM, Jin XM. Quantum transport in fractal networks. Nature Photon 2021;15(9):703–10.
[58] Manna S, Nandy S, Roy B. Higher-order topological phases on fractal lattices. Phys Rev B 2022;105:L201301.